Morse-type Frenkel-Kontorova model

Chung-I Chou,[1] Choon-Lin Ho,[1] Bambi Hu,[2,3] and Hsuan Lee[1]
[1]*Department of Physics, Tamkang University, Tamsui, Taiwan 25137, Republic of China*
[2]*Department of Physics and Centre for Nonlinear and Complex Systems, Hong Kong Baptist University, Kowloon, Hong Kong*
[3]*Department of Physics, University of Houston, Houston, Texas 77204-5506*
(Received 19 May 1997; revised manuscript received 25 August 1997)

We have investigated a generalized Frenkel-Kontorova model with a Morse-type potential which can change from a convex function to a nonconvex one as the nonlinearity parameter σ is reduced. For small enough σ, there appear in the phase diagram nonconvex phases in which at least one pair of atoms is influenced by the nonconvex part of the Morse potential. There are no incommensurate states in the nonconvex phases. For $\sigma>0.35$, a devil's staircase along the critical points of the Aubry transitions of all incommensurate states can be constructed. We studied the universality of the Hausdorff dimension of the devil's staircase, and of some critical exponents relevant to the Aubry transitions. [S1063-651X(98)14302-7]

PACS number(s): 05.45.+b, 64.70.Rh, 05.70.Jk

I. INTRODUCTION

Many condensed-matter systems, such as charge-density waves, magnetic spirals, and adsorbed monolayers, exhibit the structures of commensurate and incommensurate states, as a result of two or more competing interactions in the systems. The main features of such modulated structures are well modeled by the Frenkel-Kontorova (FK) model [1,2].

The FK model describes a chain of atoms subjected to an external periodic potential. The Hamiltonian of the FK model can be divided into two parts. One part is the energy which is due to the interatomic interactions, and the other is the energy of the atoms in the external periodic potential. For the standard FK model, the chain of atoms is connected by harmonic springs and subjected to an external sinusoidal potential. The Hamiltonian of the standard FK model is given by

$$H=\sum_i \left[W_i(x_{i+1}-x_i)+V(x_i)\right] = \sum_i \left[\frac{1}{2}(x_{i+1}-x_i-\gamma)^2+\frac{k}{(2\pi)^2}(1-\cos 2\pi x_i)\right]. \tag{1}$$

Here $W_i(x_{i+1}-x_i)$ is the potential of the interaction between two nearest atoms, $V(x_i)$ the external sinusoidal potential, x_i the position of the ith atom, γ the neutral length of the spring, and k the rescaled strength of the external potential compared to that of the spring potential. This seemingly simple one-dimensional model turns out to have very interesting structures. The phase diagrams of the standard FK model and various phase transitions occurring in the system have been thoroughly studied in previous works [3–7].

In order to better model the real systems, many researchers had considered FK models with more complicated forms of potentials. Some modified the forms of the external periodic potential [8,9], while others changed the forms of the interaction between atoms [6,10–15].

Of the works which considered modified forms of interatomic interactions, Refs. [6,10–13] changed the type of interactive potential from convex functions to nonconvex ones. These works were mainly concerned with the many complicated phase diagrams and phase transitions induced by the nonconvex potentials, and thus did not discuss the important pinning-depinning phase transition along the incommensurate states (the so-called Aubry transition) [4]. References [14, 15] considered convex potentials of the Toda and the cosh type. Multifractal structures and local critical exponents of the Aubry transition are studied in these works, but the phase diagrams found were simply smooth deformations of that of the standard FK model.

In this work, we shall consider a generalized FK model with a nonconvex interatomic potential having the form of a modified Morse potential [16]. This potential is chosen not only because it represents the interatomic interaction better than the simple harmonic potential does, but also because it can change gradually from a convex function to a nonconvex one as the nonlinearity parameter σ of this potential changes. This enables us to see how the complicated phase structures emerge, and how the Aubry transitions are affected as the nonconvex interaction sets in.

What we found can be briefly summarized below. For large enough σ, the phase diagrams of this model are simply smooth deformations of the phase diagram in the standard FK model. But as σ decreases, nonconvex phases begin to emerge. These are the phases in which at least one pair of atoms is influenced by the nonconvex part of the Morse potential. Incommensurate states do not exist in the nonconvex phases, indicating that these states are destroyed by the nonconvex interaction. For σ smaller than a critical value, which is found to be 0.35, the Aubry transitions do not exist in some part of the phase diagram. For $\sigma>0.35$, a devil's staircase along the critical points of the Aubry transitions of all incommensurate states can be constructed. The generalized fractal dimension and the singularity spectrum vary slightly as σ changes in this range. The Hausdorff dimension, however, is the same as those found in the standard, Toda-, and cosh-type Frenkel-Kontorova models (for a wide range of

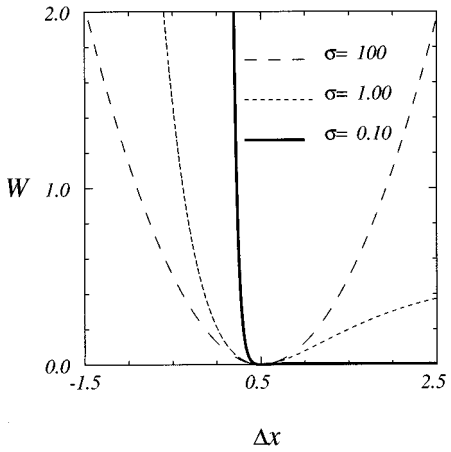

FIG. 1. Plots of the Morse potential W in Eq. (2) for various σ ($\gamma=0.5$).

nonlinearity parameters in the latter two models). Critical exponents of the gap in the phonon spectrum, the correlation length, and the Peierls-Nabarro barrier are truly universal in these models, whenever Aubry transitions exist.

This paper is organized as follows. Our model is introduced in Sec. II. In Sec. III we briefly summarize the numerical methods employed in the determination of the ground state configurations. Section IV presents our results of phase diagrams. The Aubry transition is discussed in Sec. V. Global and local behaviors are studied in Secs. VI and VII, respectively. Section VIII concludes the paper.

II. DEFINITION OF THE MODEL

The model we consider here is defined by replacing the interatomic potential $W(x_{i+1}-x_i)$ in Eq. (1) by the following modified Morse potential:

$$W_i=\frac{\sigma^2}{2}\,[e^{-(x_{i+1}-x_i-\gamma)/\sigma}-1]^2. \tag{2}$$

Here σ is a nonlinearity parameter. By changing the value of σ, one can change the Morse potential W_i from a convex function to a nonconvex one. We show in Fig. 1 the forms of W in different limits. When σ approaches to infinity, Eq. (2) reduces to the harmonic potential:

$$W(\Delta x)\rightarrow\tfrac{1}{2}(\Delta x-\gamma)^2,\quad \sigma\rightarrow\infty \tag{3}$$

where $\Delta x\equiv x_{i+1}-x_i$. In this limit, the Morse FK model becomes the standard FK model. When σ is not too large, the potential $W(\Delta x)$ is like the original Morse potential:

$$W(\Delta x)\rightarrow\begin{cases}\infty, & \Delta x\ll\gamma\\ \sigma^2/2, & \Delta x\gg\gamma\\ 0, & \Delta x=\gamma.\end{cases} \tag{4}$$

Here the potential $W(\Delta x)$ is a nonconvex function. When σ approaches zero, the potential $W(\Delta x)$ is like the potential of a hard rod:

$$W(\Delta x)\rightarrow\begin{cases}\infty, & \Delta x<\gamma\\ 0, & \Delta x\geq\gamma\end{cases}. \tag{5}$$

Any atom on the edge of the rod cannot be compressed but can be easily separated.

Let us consider the force F between the atoms. The relation of the force and the distance of two nearest atoms is given by

$$F=-\frac{\partial W}{\partial(\Delta x)}=\sigma[e^{-2(\Delta x-\gamma)/\sigma}-e^{-(\Delta x-\gamma)/\sigma})]. \tag{6}$$

The restoring force F between atoms increases without limit when the distance of two nearest atoms is shorter than the natural length of the spring ($\Delta x<\gamma$). That means the spring is hard to compress.

However, when the distance of two nearest atoms is longer than the natural length of the spring ($\Delta x>\gamma$), there exists a limiting value of F, $F_c=-\sigma/4$, at the inflection point $\Delta x=\Delta x_I\equiv\gamma+\sigma\ln 2$, so that the two atoms can be separated by an external force with a magnitude greater than $|F_c|$. The potential $W(\Delta x)$ is a convex function when two atoms are not separated beyond the inflection point. When σ increases, the range where $W(\Delta x)$ is a convex function increases. As σ decreases, Δx_I as well as $|F_c|$, the force which can break up the chain, also decreases. But the force required to compress the chain increases rather quickly.

We are interested in the phase diagrams and the related global and local properties of the model. To do that one must first obtain the ground state configurations of the system for given values of the defining parameters. This is done numerically.

III. NUMERICAL METHODS

The phase diagram consists of commensurate and incommensurate ground states in the parameter space of k and γ. The ground state is defined to be the configuration of atoms $\{x_i\}$ which has the smallest value of average energy per atom for a given set of the control parameters (k,σ,γ). The ground state could be commensurate or incommensurate. To distinguish these states, one has to define a winding number ω corresponding to the state, which is the ratio of the mean distance between successive atoms and the period of the external potential. Since the period of the external potential in our model has been set to unity, the winding number is simply the mean distance between successive atoms,

$$\omega=\lim_{n\rightarrow\infty}\frac{x_n-x_0}{n}. \tag{7}$$

If the winding number ω is a rational number, i.e., $\omega=P/Q$ (P and Q both being integers), the atoms are periodic. The system is said to be in a commensurate state. If the winding number ω is irrational, the state of the system is incommensurate.

We employed two different methods to determine the ground state configurations. Since the Morse potential is nonconvex, we use the method of effective potential in the construction of the phase diagrams in order to eliminate unwanted metastable states. But in the studies of various global and local properties of the system, methods that are based on the equilibrium condition are used for better accuracy. Both methods are briefly summarized below.

A. The method of effective potential

To construct the phase diagrams of the model, one must first obtain the ground state configurations. Since the Morse potential W_i in our model is nonconvex, the method of effective potential developed in [10] is essential. This method is equivalent to solving a minimax eigenvalue equation

$$\lambda + R(u) = V(u) + \min_{u'}[W(u-u') + R(u')]. \tag{8}$$

Here $R(u)$ is the effective potential, λ is the average energy per atom, $V(u)$ is the external potential, and $W(u-u')$ is the potential of the interaction between atoms. After the effective potential is computed, we then obtain the ground state configurations $\{x_i\}$ by means of a certain one-dimensional map, the so-called τ map [10]. And the winding number ω is obtained by comparing the ground state configurations $\{x_i\}$. One may also use the effective potential $R(u)$ to compute the total effective potential in order to determine the winding number.

The advantage of this method is that it needs only the Hamiltonian of the FK model to find the true ground state configurations, and that it works for both convex and nonconvex potentials. Other methods may give metastable states in the presence of nonconvex potentials. The method has, however, the following drawbacks. (1) The precision of the ground state configurations depends on the grid size N employed. Two atoms cannot be distinguished if their distance is smaller than $1/N$. (2) The denominator Q of the rational winding number ($\omega = P/Q$) must be smaller than N. (3) Because of the limit in precision in the ground state configurations mentioned in point (1), one cannot obtain accurate values of quantities, such as critical exponents, which are relevant to the Aubry transitions. (4) This method is time consuming.

B. The methods based on the equilibrium condition

We can use Aubry's gradient method [4] to write down a system of differential equations for the forces acting on the atoms:

$$-\frac{\partial H_i}{\partial x_i} = \frac{dx_i}{d\tau}. \tag{9}$$

They must satisfy the periodic condition $x_{i+Q} = x_i + P$. Using the initial condition $x_i = x_0 + iP/Q$, we can find the ground state configuration $\{x_i\}$. In view of the fact that the ground state must satisfy the equilibrium condition $\partial H_i/\partial x_i = 0$, Schellnhuber and collaborators [17] suggested a Newton's method which searches directly for the solution of $\partial H_i/\partial x_i = 0$. By using this method, we just need to consider the periodic condition $x_{i+Q} = x_i + P$ and the initial condition $x_i(0) = [iP/Q]$, where [ ] means the integral part.

The advantages of these methods are that they are faster and more accurate than the method of effective potential is. They have, however, the following disadvantages: (1) they require the periodic condition $x_{i+Q} = x_i + P$, which means the winding number must be determined beforehand; (2) these methods very often give metastable configurations when there exists nonconvex interaction as in our model.

Our strategy is therefore to first use the method of effective potential to search for the ground state configurations needed in the construction of the phase diagrams, and then use the method of equilibrium condition for a more accurate determination of the values of x_i's which are required in the study of the Aubry transition.

IV. PHASE DIAGRAMS

In this section we shall study the phase diagrams of the model as the nonlinearity parameter σ is changed. The ground states are determined by the method of effective potential with a grid size N varying from 100 to 1000. The results we obtained are as follows.

When σ is very large ($\sigma \gg 1$), the Morse FK model reverts to the standard FK model. Naturally, the phase diagrams of the Morse FK model are essentially the same as that of the standard FK model. For any given rational winding number ω, there is a corresponding commensurate area (the Arnold tongue) in the phase diagram in which ω is constant. Between any two tongues there is a gap that contains incommensurate states as well as higher-order commensurate states. The winding numbers of the tongues are comprised of all the rational numbers between 0 and 1.

As σ decreases ($\sigma \leqslant 1$), the tongues on the upper side of the phase diagram expand gradually to the left, but the winding numbers remain the same (see Fig. 2). When σ decreases further ($\sigma < 0.5$), the tongues that are constructed by winding numbers $1/Q$ ($Q = 1,2,\ldots$) expand rather quickly on their left edges, and begin to cover the tongues with $\omega = P/Q$, where $P \neq 1$ (see Fig. 3).

When σ decreases further ($\sigma < 0.35$), the tongues that are constructed by winding numbers $1/Q$ are getting larger, and nonminimal periodic configurations, such as states with $\omega = n/nQ$ ($n, Q = 1,2,\ldots$), begin to appear (see Fig. 4). The phase diagram is very similar to the phase diagram of the sine-Lennard-Jones system [18]. The upper part of the phase diagram is now filled only with tongues of winding numbers $1/Q$ and areas with $\omega = n/nQ$. There are no incommensurate states with irrational winding numbers in this region. As will be seen below, the disappearance of the incommensurate states has to do with the nonconvex part of the Morse potential. It is seen that tongues with smaller values of Q have larger areas. The areas of the $\omega = n/n$ phase increase when σ decreases, but the areas of the $\omega = n/2n$ states will be covered by the tongues $\omega = 1/1$. The lower part of the phase diagram still consists of the tongues of winding numbers $\omega = P/Q$. This is the part that expands to the phase diagram of the standard FK model as $\sigma \to \infty$.

To better understand the structures of the phase diagram, it is useful to follow the definition in [19] (see also [12]). We shall call a phase ''nonconvex'' if at least one pair of atoms experiences the nonconvex part of the Morse potential $W(\Delta x)$. In this case, at least one pair of the atoms is separated beyond the inflection point of the Morse potential, i.e., $\Delta x > \Delta x_I = \gamma + \sigma \ln 2$. If none of the atoms uses the nonconvex part of the potential, the phase is called ''convex.''

We indicate by shaded areas the nonconvex phases in Figs. 2–4. It is seen that nonconvex phases only occur in the commensurate states with $\omega = 1/Q$ and n/nQ in the upper part of the phase diagram. As discussed before, this part of

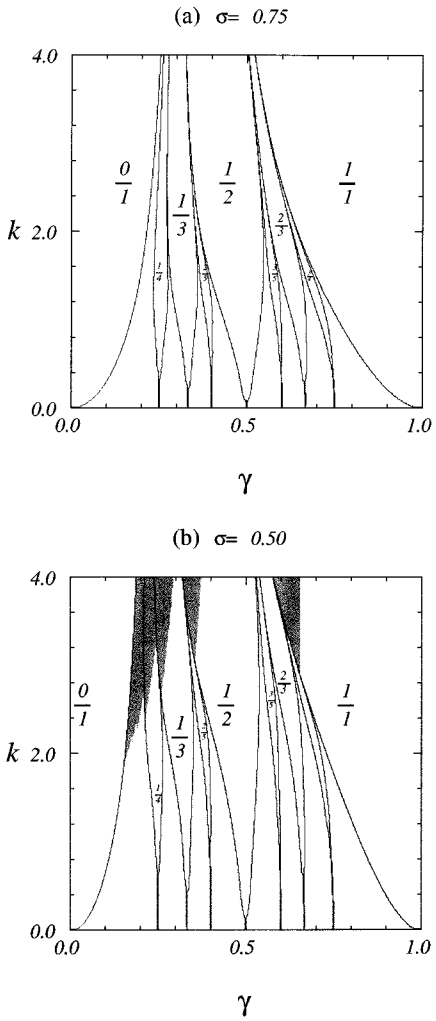

FIG. 2. Phase diagram of the Morse FK model for $\sigma=0.75$ and 0.50. Shaded regions represent nonconvex phases.

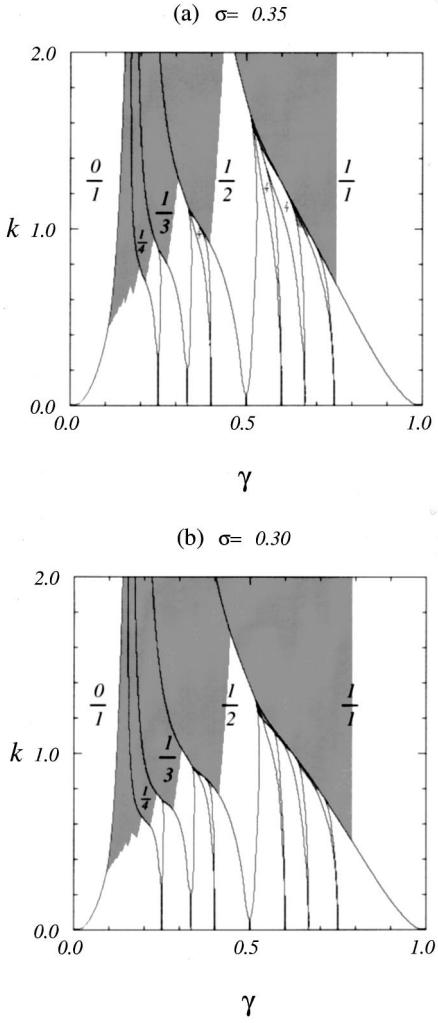

FIG. 3. Phase diagram of the Morse FK model for $\sigma=0.35$ and 0.30. Shaded regions represent nonconvex phases.

the diagram expands rather quickly over the part with all rational and irrational winding numbers as σ decreases. And since for small σ the nonconvex part of the Morse potential is more easily experienced by the atoms, one reaches the conclusion that nonconvex interaction destroys incommensurate structures.

To conclude this section, let us mention an interesting observation about the rate of contraction of the boundary curve between the convex and nonconvex phases for small σ. Numerically we find that the values of k on this curve scale as σ^2, i.e., $k\sim\sigma^2$, as $\sigma\rightarrow 0$.

V. THE AUBRY TRANSITIONS

In his studies of the standard FK model, Aubry [4] showed that when the winding number ω is rational, the system of the FK model is always pinned. But when the winding number ω is irrational, on the curve of incommensurate state in the parameter space of k and γ, there exists a critical point $k_c(\omega)$ such that when $k<k_c(\omega)$, the system is unpinned; and when $k>k_c(\omega)$, the system becomes pinned. This pinning-depinning transition in the FK model is called the Aubry transition. We shall also study such transitions in our model.

As we have seen in the preceding section, for large enough σ in our model, the phase diagrams are smooth deformations of that in the standard FK model. We can thus study how the Aubry transitions are affected by the change in the σ. When σ becomes small, the nonconvex part of the Morse potential becomes important. It has the effect of destroying the incommensurate states. Therefore, for small σ in our model, there are no Aubry transitions in those parts of the phase diagram which consist of the nonconvex phases.

To study the Aubry transitions one must have a more accurate construction of the phase diagrams. As mentioned before, we employ for this purpose the method of equilibrium condition to locate the periodic ground states. The phase diagram is then obtained by means of the Farey tree construction [6,14,15]. In the nth Farey generation, there are $2^{n-1}+1$ rational numbers (hence tongues) in the interval [0,1]. The curves of incommensurate states can also be constructed using the nth Farey generation. For a given irrational winding number ω^*, we can find two rational winding numbers ω' and ω'' that satisfy $\omega'<\omega^*<\omega''$ from the nth Farey generation to approximate ω^*. When n becomes infinite, the differences in these winding numbers will disappear ($\omega'\cong\omega^*\cong\omega''$). The average energy per atom for these

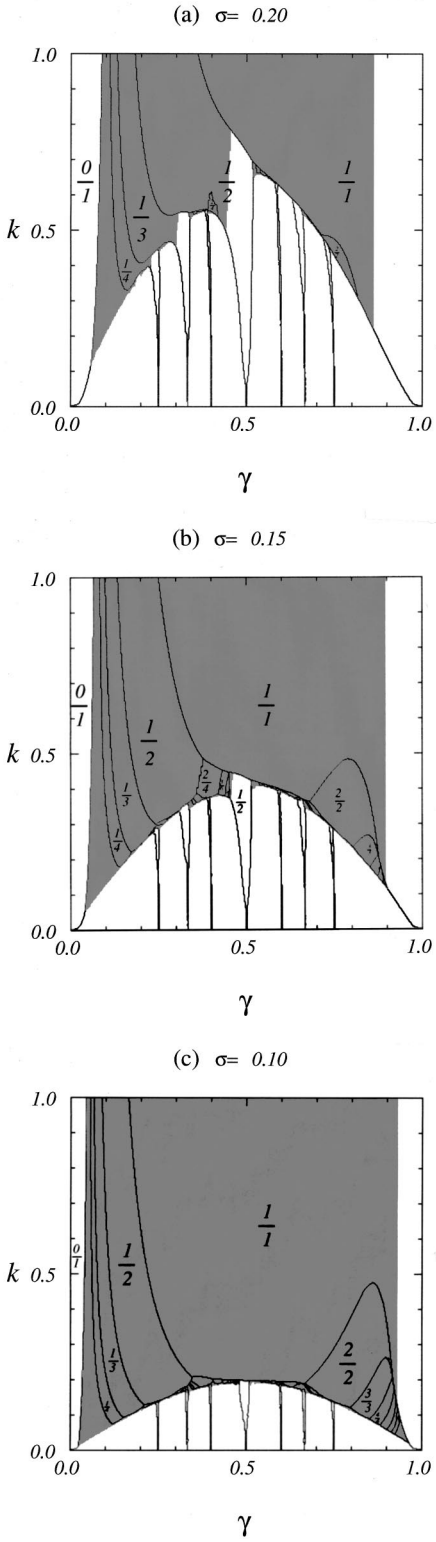

FIG. 4. Phase diagram of the Morse FK model for $\sigma=0.20$, 0.15, and 0.10. Shaded regions represent nonconvex phases.

winding numbers will be the same, $\overline{H(\omega')}=\overline{H(\omega^*)}=H(\omega'')$. Solving these equations one can find the value of γ for given values of σ and k. For a fixed value of σ, the points (γ,k) then constitute the curve of incommensurate state corresponding to the irrational winding number ω^*,

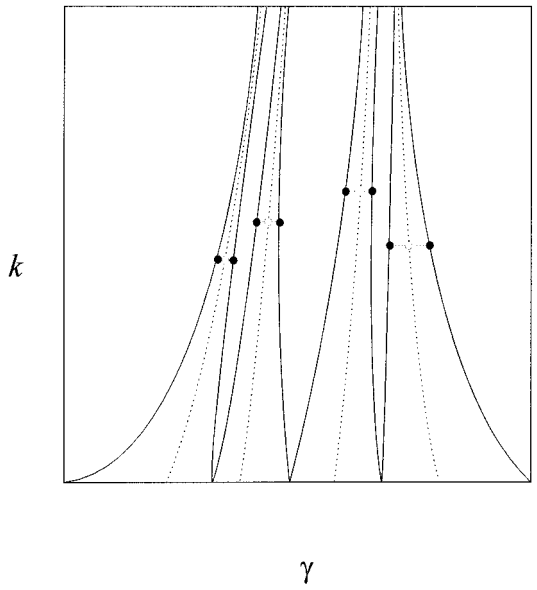

FIG. 5. Schematic diagram for the constructions of curves of incommensurate states (the dotted curves) and the critical points (the circles). The black dots represent points on the edges of the Arnold tongues which are at the same heights as the neighboring critical points. The edges of the steps in the devil's staircase are determined by the black dots on the two edges of each tongue.

depicted as a dotted curve in Fig. 5.

The next step is to calculate the critical value $k_c(\omega)$, represented by a small circle in Fig. 5, of the Aubry transition along the curve of an incommensurate state. To this end the powerful method of Greene [20,21] is used. This method requires one to first rewrite the equilibrium condition $\partial H_i/\partial x_i=0$ as a two-dimensional map,

$$y_{i+1}=f(x_i,y_i),$$

$$x_{i+1}=g(x_i,y_i). \tag{10}$$

Unlike the standard FK model, such a map is not unique for the Morse FK model. The equilibrium condition for our model is

$$\frac{\partial H_i}{\partial x_i}=0=\sigma[e^{-2(x_{i+1}-x_i-\gamma)/\sigma}-e^{-(x_{i+1}-x_i-\gamma)/\sigma}]-\sigma[e^{-2(x_i-x_{i-1}-\gamma)/\sigma}-e^{-(x_i-x_{i-1}-\gamma)/\sigma}]+\frac{k}{2\pi}\sin 2\pi x_i. \tag{11}$$

Defining $y_{i+1}=x_{i+1}-x_i$, we obtain two possible maps which are equivalent to Eq. (11). The first map is

$$y_{i+1}=\gamma-\sigma\ \ln\{\tfrac{1}{2}+\sqrt{u_i}\},$$

$$x_{i+1}=x_i+y_{i+1}, \tag{12}$$

with the Jacobian

$$M_i \equiv \begin{pmatrix} \frac{\partial f}{\partial y_i} & \frac{\partial f}{\partial x_i} \\ \frac{\partial g}{\partial y_i} & \frac{\partial g}{\partial x_i} \end{pmatrix} = \frac{1}{u_i + \sqrt{u_i}/2} \begin{pmatrix} e^{-2(y_i-\gamma)/\sigma} - \frac{1}{2} e^{-(y_i-\gamma)/\sigma} & \frac{1}{2} k \cos 2\pi x_i \\ e^{-2(y_i-\gamma)/\sigma} - \frac{1}{2} e^{-(y_i-\gamma)/\sigma} & u_i + \frac{1}{2}\sqrt{u_i} + \frac{1}{2} k \cos 2\pi x_i \end{pmatrix}. \tag{13}$$

Here $u_i \equiv [e^{-(y_i-\gamma)/\sigma} - \frac{1}{2}]^2 - k \sin(2\pi x_i)/2\pi\sigma$. From Eq. (11), u_i can also be expressed as $u_i = [e^{-(y_{i+1}-\gamma)/\sigma} - \frac{1}{2}]^2$. Hence u_i is non-negative.

The second map is

$$y_{i+1} = \gamma - \sigma \ln\{\tfrac{1}{2} - \sqrt{u_i}\},$$
$$x_{i+1} = x_i + y_{i+1}, \tag{14}$$

and the corresponding Jacobian is

$$M_i' = \frac{1}{u_i - \sqrt{u_i}/2} \begin{pmatrix} e^{-2(y_i-\gamma)/\sigma} - \frac{1}{2} e^{-(y_i-\gamma)/\sigma} & \frac{1}{2} k \cos 2\pi x_i \\ e^{-2(y_i-\gamma)/\sigma} - \frac{1}{2} e^{-(y_i-\gamma)/\sigma} & u_i - \frac{1}{2}\sqrt{u_i} + \frac{1}{2} k \cos 2\pi x_i \end{pmatrix}. \tag{15}$$

From the two maps (12) and (14), one easily sees that in the second map the distance between any two neighboring atoms is longer than the distance of the inflection point $\gamma + \sigma \ln 2$, and hence map (14) does not give configurations in the convex phases. So we only use the first map (12) in Greene's method to compute the critical point $k_c(\omega)$.

VI. GLOBAL BEHAVIORS OF PHASE TRANSITION OF INCOMMENSURATE STATES

There are two kinds of properties which are of interest in the Aubry transitions. One is the global behavior, which concerns the structures constituted by all of the critical points $k_c(\omega)$. The other is the local behavior, which pertains to the critical behaviors at the critical point $k_c(\omega)$ of any incommensurate state. In this section, we shall study the global behavior first. The local behavior is considered in the next section.

A. Critical lines

The critical line is defined to be the collection of the critical points $k_c(\omega)$ for all irrational winding number ω. Figure 6 shows critical lines for various defining parameters of the model. It can be seen that the critical lines vary greatly as σ changes. And when σ becomes small ($\sigma < 0.35$), some critical points $k_c(\omega)$ are ''eaten'' by the nonconvex phases on the phase diagram. As mentioned before, there are no Aubry transitions on these curves of the incommensurate states in these parts of the phase diagram. In the following we shall be interested in the global properties of critical lines which consist of critical points $k_c(\omega)$ of all incommensurate states. That means only phase diagrams for $\sigma \geqslant 0.35$ will be considered.

B. Devil's staircases

The devil's staircase on the critical line $k_c(\omega)$ is formed by considering the winding number ω as a function of the parameter γ (see Fig. 5). This function contains only steps, each of them representing a stable commensurate state. Magnification of any part of the curve (not within a step) will reproduce the original curve [6]. The devil's staircases are multifractals. Figure 7 presents some of the devil's staircases in our model.

C. Multifractal structures

To understand the multifractal structures of the devil's staircases, we follow [15] and determine the Hausdorff dimension D_0, the generalized fractal dimension D_q, and the singularity spectrum $f(\alpha)$.

1. Hausdorff dimension

By the definition of Hausdorff dimension D_0, we can construct a partition function from the nth Farey generation. Let l_i be the width of the ith piece. The partition function is

$$\Gamma^{(n)}(D) = \sum_{i=1}^{2^{n-1}} l_i^D. \tag{16}$$

When n approaches infinity, one has $\Gamma(D) = \infty$ if $D > D_0$, and $\Gamma(D) = 0$ if $D < D_0$. One may choose a finite positive constant B and determine D_0 by solving the equation $\Gamma^{(n)}(D_0) = B$. In order to improve on convergence in our computation, we apply instead the ratio trick [22] by considering the ratio of two partition functions in different Farey generations:

$$\frac{\Gamma^{(n+1)}(D_0)}{\Gamma^{(n)}(D_0)} = 1. \tag{17}$$

The convergence increases as n increases. We used $n = 9$ in our calculations.

We compute D_0 for σ ranging from $\sigma = 100$ to 0.35, and find that the values of the Hausdorff dimension in these cases are the same within computational error. It is 0.845 ± 0.002, which is also the same as that found for the standard FK model, the cosh FK model (when the nonlinearity parameter

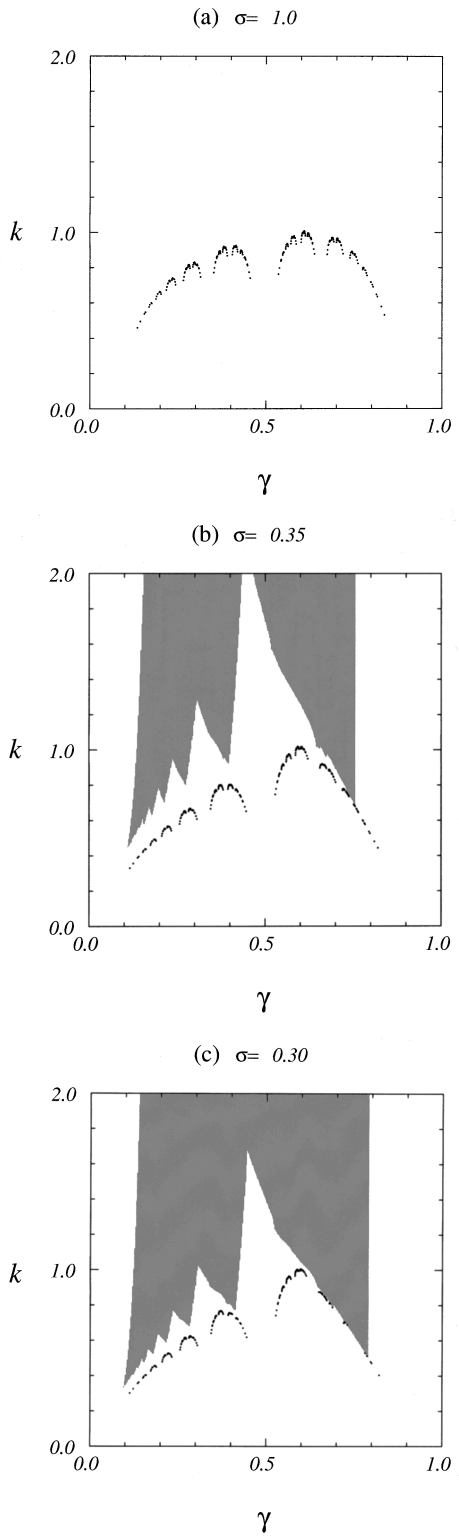

FIG. 6. Critical line of the Morse FK model for $\sigma=1.0$, 0.35, and 0.30. Shaded regions represent nonconvex phases.

σ of this model is not less than 0.5) [15], and the Toda FK model (when the nonlinearity parameter β, defined in [14], is not greater than one) [23].

2. Multifractal properties

Multifractal properties include the generalized fractal dimension D_q and the singularity spectrum $f(\alpha)$. Let l_i again

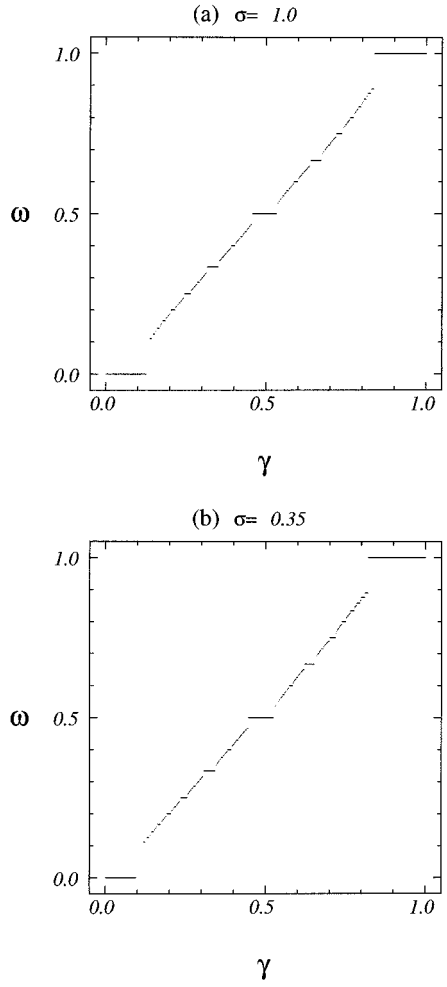

FIG. 7. Devil's staircase of the Morse FK model for $\sigma=1.0$ and 0.35. Staircases up to the ninth Farey generation are shown.

be the width of the ith piece, and m_i the difference of the winding numbers of two neighboring steps:

$$m_i=\omega_{i+1}-\omega_i. \tag{18}$$

The partition function of the multifractal can be written in nth Farey generation as [22]

$$\Gamma^{(n)}(q,\tau)=\sum_{i=1}^{2^{n-1}}\frac{m_i^q}{l_i^{\tau(q)}}. \tag{19}$$

Again, one may choose a finite positive constant B and determine the relation between $\tau(q)$ and q by solving the equation $\Gamma^{(n)}(q,\tau)=B$. As in the preceding subsection, we prefer to determine $\tau(q)$ by considering the ratio of two partition functions in different Farey generations,

$$\frac{\Gamma^{(n+1)}(q,\tau)}{\Gamma^{(n)}(q,\tau)}=1. \tag{20}$$

Again, we used $n=9$ in our calculations. Once $\tau(q)$ is obtained, we can compute $\alpha(q)$ as

$$\alpha(q)=\frac{d}{dq}\tau(q). \tag{21}$$

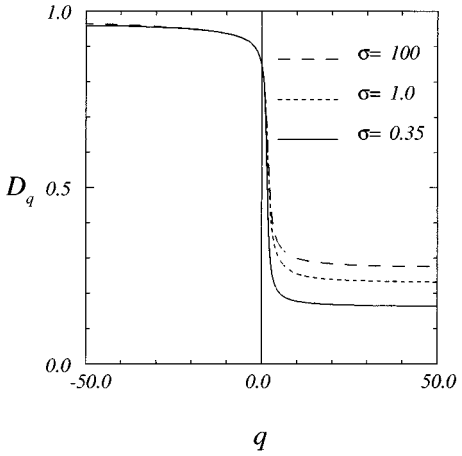

FIG. 8. Generalized dimension D_q of the devil's staircase for $\sigma=100$, 1.0, and 0.35.

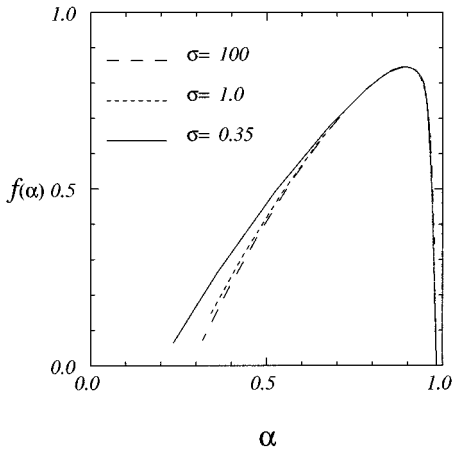

FIG. 9. Singularity spectrum $f(\alpha)$ of the devil's staircase for $\sigma=100$, 1.0, and 0.35.

And then the generalized fractal dimension D_q and the singularity spectrum $f(\alpha)$ can be calculated:

$$D_q=\frac{\tau(q)}{q-1}, \tag{22}$$

$$f(\alpha)=q\alpha(q)-\tau(q). \tag{23}$$

Our numerical results are shown in Figs. 8 and 9. As σ decreases, D_∞ decreases but both the Hausdorff dimension $D_0=0.845\pm0.002$ and $D_{-\infty}$ (we find $D_{-50}=0.960\pm0.005$) remain practically unchanged. Representative values for D_∞ are $D_{50}=0.16\pm0.02$, 0.22 ± 0.02, and 0.26 ± 0.05 for $\sigma=0.35$, 1, and $\sigma\geqslant100$, respectively.

We can see the same behaviors in the singularity spectrum $f(\alpha)$. As σ decreases, the minimum of α decreases but the maximum of α and of $f(\alpha)$ remain practically unchanged.

From the above results, we see that while the general shapes of the curves of D_q and $f(\alpha)$ vary in different generalized FK models, there is still universality in the Hausdorff dimension D_0 [which equals the maximum of $f(\alpha)$] in the standard FK, the Toda FK ($\beta\leqslant1$), the cosh FK ($\sigma\geqslant0.5$), and the Morse FK ($\sigma\geqslant0.35$) model.

VII. LOCAL BEHAVIORS OF PHASE TRANSITION OF INCOMMENSURATE STATES

We now turn to discuss critical behaviors at the critical point $k_c(\omega)$ of incommensurate states. The winding number associated with the largest critical point $k_c(\omega)$ is the golden mean number $\omega=(\sqrt{5}-1)/2$, which has a representation in continued fractions as $\omega=[0,1,1,1,1,\ldots]$. This corresponds to the breakup of the last Kolmogorov-Arnol'd-Moser (KAM) torus. We shall compute the critical exponents of the Aubry transition along this curve for different values of σ.

A. The gap in the phonon spectrum

Consider a small vibration $\epsilon_i(t)$ of the ith atom around the equilibrium position x_i,

$$x_i(t)=x_i+\epsilon_i(t). \tag{24}$$

Then the linearized equation of motion for small vibration is given by

$$\epsilon_i(t)=-\sum_j \frac{\partial^2 H(\{x_i\})}{\partial x_i\partial x_j}\,\epsilon_j(t), \quad i,j=1,2,\ldots,Q. \tag{25}$$

For the Morse FK model,

$$\frac{\partial^2 H}{\partial x_i\partial x_j}=\begin{cases}-2e^{-2\delta_{i+1}}+e^{-\delta_{i+1}}, & j=i+1\\ 2e^{-2\delta_{i+1}}-e^{-\delta_{i+1}}+2e^{-2\delta_i}-e^{-\delta_i}+k\,\cos 2\pi x_i, & j=i\\ -2e^{-2\delta_i}+e^{-\delta_i}, & j=i-1\end{cases} \tag{26}$$

where $\delta_i\equiv(x_i-x_{i-1}-\gamma)/\sigma$.

The Fourier transform in time t of Eq. (26) gives

$$0=(-2e^{-2\delta_i}+e^{-\delta_i})\epsilon_{i-1}+(2e^{-2\delta_{i+1}}-e^{-\delta_{i+1}}+2e^{-2\delta_i}-e^{-\delta_i}+k\,\cos 2\pi x_i-\Omega^2)\epsilon_i+(-2e^{-2\delta_{i+1}}+e^{-\delta_{i+1}})\epsilon_{i+1},$$
$$i=1,2,\ldots,Q. \tag{27}$$

The phonon spectrum $\{\Omega_i\}$ is obtained by solving this $Q\times Q$ matrix equation (27). The gap in the phonon spectrum Ω_G is defined to be the lowest phonon frequency in the system, $\Omega_G=\min\{\Omega_i\}$. For $k<k_c$, the ground state of the chain is in a sliding mode and therefore $\Omega_G=0$. As $k>k_c$, a gap Ω_G in the phonon spectrum appears and the critical behavior of Ω_G can be characterized by the exponent χ [7],

$$\Omega_G(k) \sim (k-k_c)^{\chi}. \tag{28}$$

We have calculated χ for values of σ ranging from 0.35 to 100. The result is $\chi = 1.02 \pm 0.01$, which is independent of σ and k_c.

B. The correlation length

The correlation length ξ is defined to be the distance over which a perturbation ϵ_i of the ith atom propagates along the chain. An infinitesimal perturbation ϵ_i at x_i will cause a displacement ϵ_j at x_j, where

$$\epsilon_j \sim \exp(-|x_j - x_i|/\xi)\,\epsilon_i. \tag{29}$$

It has been shown [7] that the correlation length ξ is the inverse of the Lyapunov exponent λ, $\xi = 1/\lambda$. The Lyapunov exponent λ can be obtained from the eigenvalue of the Jacobian matrix $M = M_Q M_{Q-1} \cdots M_1$, where M_i are given by Eq. (13).

For $k < k_c$, the Lyapunov exponent λ is equal to zero, $\lambda = 0$. For $k > k_c$, the Lyapunov exponent λ scales as

$$\lambda \sim (k-k_c)^{\nu}. \tag{30}$$

For the range of σ we considered, the critical exponent ν is found to be $\nu = 0.99 \pm 0.01$, which is also independent of σ and k_c.

C. The Peierls-Nabarro barrier

The Peierls-Nabarro (PN) barrier of a ground state is defined to be the minimal energy barrier that must be overcome to translate continuously the chain of atoms on the periodic potential.

For $k < k_c$, the PN barrier is equal to zero, which means the chain of atoms can slide without any extra energy. For $k > k_c$, the PN barrier is nonvanishing and scales as

$$E_{\mathrm{PN}} \sim (k-k_c)^{\Psi}, \tag{31}$$

where Ψ is the critical exponent related to E_{PN}.

The value of the critical exponent Ψ is found to be $\Psi = 3.00 \pm 0.02$ for the values of σ we considered. As with the other two exponents, it is independent of σ and k_c.

VIII. SUMMARY

In this paper we have investigated a generalized FK model with a Morse-type interatomic action. The Morse potential we considered can change from a convex function to a nonconvex one as the nonlinearity parameter σ is reduced. We studied how such changes affect the phase diagrams, the critical lines, the multifractal structures, and local critical behaviors in this model. We found that the phase diagram is qualitatively different from the phase diagram of the standard FK model. There could exist nonconvex phases in which at least one pair of atoms is influenced by the nonconvex part of the Morse potential. There are no incommensurate phases in the nonconvex portion of the phase diagrams. Hence nonconvex interaction destroys incommensurate structures. It is found that when $\sigma < 0.35$, some critical points $k_c(\omega)$ are ''eaten'' by the nonconvex area in the phase diagram. The critical lines become incomplete in these cases. We therefore studied the multifractal structures and critical properties of the Aubry transitions only for $\sigma > 0.35$. Calculations of the local critical exponents of the Aubry transitions in this model show that these exponents are independent of σ and k_c, and that they are of the same values as the corresponding exponents in the standard, the Toda-, and the cosh-type FK model. Hence the Aubry transitions in all these four types of FK models belong to the same universality class. The Hausdorff dimension in the Morse FK model (for $\sigma \geqslant 0.35$) is also found to be the same as that found in the standard FK model. This is similar to the situation in the Toda and the cosh FK model, in which the Hausdorff dimension assumes the same value only for a certain range of the corresponding nonlinearity parameter.

ACKNOWLEDGMENTS

This work was supported in part by Republic of China Grant No. NSC 86-2112-M-032-002 (C.I.C. and C.L.H.), and in part by the Research Grants Council Grant No. RGC/96-97/10 and Faculty Research Grant Nos. FRG/95-96/II-09 and FRG/95-96/II-92 (B.H.).

[1] Y. I. Frenkel and T. Kontorova, Zh. Eksp. Teor. Fiz. **8**, 1340 (1938) [Sov. Phys. JETP **13**, 1 (1938)].
[2] F. C. Frank and J. H. van der Merwe, Proc. R. Soc. London, Ser. A **198**, 205 (1949).
[3] P. Bak, Rep. Prog. Phys. **45**, 587 (1982).
[4] S. Aubry, in *Solitons and Condensed Matter Physics*, edited by A. R. Bishop and T. Schneider (Springer-Verlag, Berlin, 1978); J. Phys. (Paris) **44**, 147 (1983); Physica D **7**, 240 (1983); **8**, 381 (1983).
[5] R. S. MacKay, Physica D **50**, 71 (1991); Ph.D. thesis, Princeton University, 1982.
[6] O. Biham and D. Mukamel, Phys. Rev. A **39**, 5326 (1989).
[7] M. Peyrard and S. Aubry, J. Phys. C **16**, 1593 (1983); L. de Seze and S. Aubry, *ibid.* **17**, 389 (1984).
[8] J. Shi and B. Hu, Phys. Rev. A **45**, 5455 (1992).
[9] H. Johannesson, B. Schaub, and H. Suhl, Phys. Rev. B **37**, 9625 (1988).
[10] R. B. Griffiths and W. Chou, Phys. Rev. Lett. **56**, 1929 (1986); W. Chou and R. B. Griffiths, Phys. Rev. B **34**, 6219 (1986); R. B. Griffiths, in *Fundamental Problems in Statistical Mechanics VII*, edited by H. van Beijeren (North-Holland, Amsterdam, 1990), p. 69; K. E. Bassler and R. B. Griffiths, Phys. Rev. B **49**, 904 (1994).
[11] J. E. Byrne and M. D. Miller, Phys. Rev. B **39**, 374 (1989).
[12] M. Marchand, K. Hood, and A. Caillé, Phys. Rev. B **37**, 1898 (1988).
[13] N. Coppersmith and D. S. Fisher, Phys. Rev. B **28**, 2566 (1983).

[14] B. Lin and B. Hu, J. Stat. Phys. **69**, 1047 (1992).
[15] C.-I. Chou, C.-L. Ho, and B. Hu, Phys. Rev. E **55**, 5092 (1997).
[16] P. M. Morse, Phys. Rev. **34**, 57 (1929).
[17] H. J. Schellnhuber, H. Urbschat, and A. Block, Phys. Rev. A **33**, 2856 (1986); H. J. Schellnhuber, H. Urbschat, and J. Wilbrink, Z. Phys. B **80**, 305 (1990).
[18] M. D. Miller and J. S. Walker, Phys. Rev. B **44**, 2792 (1991).
[19] C. S. O. Yokoi, L. Tang, and W. Chou, Phys. Rev. B **37**, 2173 (1988).
[20] J. M. Greene, J. Math. Phys. **20**, 1183 (1979).
[21] S. J. Shenker and L. P. Kadanoff, J. Stat. Phys. **27**, 631 (1982).
[22] T. C. Halsey, M. H. Jensen, L. P. Kadanoff, I. Procaccia, and B. I. Shraiman, Phys. Rev. A **33**, 1141 (1986).
[23] Chang-Chen Lo, M.Sc. thesis (in Chinese), Tamkang University, 1996. This thesis studies the multifractal properties of the Toda FK model defined in Ref. [14]. The devil's staircases were constructed along the critical lines, as in Refs. [6, 15] and the present paper. The devil's staircases in [14], on the other hand, were constructed at the critical golden mean value $k_c(\omega_G)$. As such, the Hausdorff dimension computed in [14] cannot be used for comparison.